RSC Advances

PAPER

View Article Online
View Journal | View Issue

Cite this: *RSC Adv.*, 2021, **11**, 39270

Hydrazone connected stable luminescent covalent–organic polymer for ultrafast detection of nitro-explosives†

Muhammad Asad,[a] Ya-Jie Wang,[a] Shan Wang,*[a] Qing-Guo Dong,[a] Lin-Ke Li,*[a] Saadat Majeed,[b] Qian-You Wang[a] and Shuang-Quan Zang[a]

Received 1st November 2021
Accepted 24th November 2021

DOI: 10.1039/d1ra08009a

rsc.li/rsc-advances

Developing promising luminescent probes for the selective sensing of nitro-explosives remains a challenging issue. Porous luminescent covalent–organic polymers are one of the excellent sensing probes for trace hazardous materials. Herein, fluorescent monomers 1,1,2,2-tetrakis(4-formyl-(1,1′-biphenyl))ethane (TFBE) and 1,3,5-benzenetricarboxylic acid trihydrazide (BTCH) were selected to build a novel hydrazone connected stable luminescent covalent–organic polymer (**H-COP**) of high stability by typical Schiff-base reaction. The N_2 sorption study, BET surface area analysis, and TGA profile indicate the porosity and stability of this **H-COP** material. Such properties of the **H-COP** material enable a unique sensing platform for nitro-explosives with great sensitivity (Ksv $\sim 10^6$ M) and selectivity up to μM. This polymer material shows attractive selectivity and sensitivity towards phenolic nitro-explosives and other common explosives among earlier reported COP-based sensors.

Introduction

Explosives detection through fluorescence quenching is a frequently used powerful tool for national security and ecological protection applications.[1–3] Hazardous materials sensing at low concentration has gained significant interest to date.[4–6] Nitro-explosives, such as dinitrotoluene (DNT), dinitrobenzene (DNB), 4-nitrophenol (4-NP), and picric acid (PA) are common industrial explosives in unexploded land mines and ordnance bases.[7,8] Nitro-explosives are relatively rare in nature and have been introduced into the environment mainly by human activities.[9–12] Some nitro-explosives are plasma and liver contaminants that could be easily taken up by human skin, lungs, and many other parts of the body.[13–15] Considerably, such compounds' presence has been proven toxic for our environment. In order to minimize their chronic exposure, favorable sensing tools are highly desirable.[16] Therefore, rapid and selective detection of explosive materials has become a major ongoing challenge.[17] In the past, the detection study of explosives was sticky on instrumental based techniques.[18–20] The instruments used in the past were large, costly, non-movable, and time-consuming, which limited their use.[21] Currently, the nitro-explosives fluorescence quenching has become powerful sensing tool due to simplicity, high selectivity, sensitivity and strong sensing process, over other techniques including ion-mobility spectrometry,[22] gas chromatography technique coupling with mass spectrometry (GC-MS),[23] surface enhanced Raman spectroscopy (SERS)[24] plasma desorption-mass spectrometry (PDMS),[25] energy dispersive X-ray diffraction (EDXRD),[26] and several techniques of spectral imaging.[27] In the last few decades, nitro-explosive detection *via* fluorescence quenching technique has offered a smart and favorable alternative tool since it contains more advantages over other conventional methods.[27–30] From the first case study of nitro-explosives *via* luminescent porous material till now, a lot of efforts have been made in this field.[31–34] So far, various luminescent materials have been widely used for explosive compounds detection, include metal–organic frameworks (MOFs), porous–organic frameworks (POFs) and numerous kinds of polymer hybrid materials.[7,35–39]

For promising sensing setups, there is a need of cost-effective, highly sensitive, and advanced luminescent probes which can reveal rapid response even at very low concentrations.[40] The covalent–organic polymer (COP) based luminescent porous materials containing low weight components and all essential characteristics including high surface area, pre-designed pore parameters, well-ordered channel structure and high stability shows effective attraction in sensing field.[41] The effective way for optimizing the targeted property of covalent polymers is the incorporation of individual functional groups.

[a]*Henan Key Laboratory of Crystalline Molecular Functional Materials, Henan International Joint Laboratory of Tumor Theranostical Cluster Materials, Green Catalysis Center, College of Chemistry, Zhengzhou University, Zhengzhou 450001, P. R. China. E-mail: shanwang@zzu.edu.cn; lilinke@zzu.edu.cn*

[b]*Institute of Chemical Sciences, Bahauddin Zakariya University, Multan, 60800, Pakistan*

† Electronic supplementary information (ESI) available. See DOI: 10.1039/d1ra08009a

Herein, we have established a novel hydrazone connected stable luminescent covalent–organic polymer (**H-COP**) *via* condensation reaction of 1,1,2,2-tetrakis(4-formyl-(1,1′-biphenyl))ethane (TFBE) and 1,3,5-benzenetricarboxylic acid trihydrazide (BTCH) units. Such binding components give potential to π-electrons, connecting sites, chemical stability, and good luminescence capabilities for promising nitro-aromatic explosives recognition. The aldehyde based ligands with strong conjugation typically used for the sensing directions and developing luminescent porous materials.[42] Covalent–organic polymers with electron-rich interiors and connection sites have been proved efficient candidates for attaining excellent consequences and sensing of electron-deficient explosive materials sensing.[43–45] This sagacity has been reasoned for the incorporation of hydrazone and aldehyde based units as stable luminescent groups into the polymer walls. This hydrazone linked stable luminescent covalent–organic polymer **H-COP** based novel sensing platform shows fascinating sensitivity and selectivity towards nitro-explosives over reported covalent–organic polymers (COPs) to date.

Experimental

Materials and methods

All the reagents were purchased of analytical grade from certified sellers and used without any further refinement. FT-IR spectra were recorded with wavelength range 4000–400 cm^{-1} using Bruker Alpha II spectrophotometer. The PXRD spectra obtained with Rigaku Miniflex diffractometer. Solid ^{13}C (CP/MAS-NMR) analysis applied *via* Bruker Ultrashield 400wb Plus. TGA analysis was conducted *via* TA Q50 thermal analyzer using sample 5 mg with range of 50–800 °C at the constant heating rate of 10 °C min^{-1} under ambient environment. Nitrogen sorption isotherms were calculated at 77 K *via* BELSORP Max II equipment using relative pressure (0–1 bar), while pore size is determined *via* NLDFT model. Scanning electron microscopic (SEM) study was investigated with Zeiss Sigma 500 microscope. Transmission electron microscopy (TEM) was explored *via* Tecnai G2 F20 S-TWIN equipment functioning at an acceleration voltage of 200 kV. UV-visible spectroscopy was performed *via* Hitachi UH4150 spectrophotometer. Photoluminescence emission and excitation spectra were recorded at ambient temperature with a HORIBA FluoroLog-3 fluorescence spectrometer, while time-resolved decay measurements were carried on HORIBA FluoroLog-3 fluorescence spectrometer equipped with a laser of 355 nm working in time-correlated single-photon counting mode (TCSPC) with a time resolution of 100 ns.

Preparation

Synthesis of H-COP. 1,1,2,2-Tetrakis(4-formyl-(1,1′-biphenyl))ethane (TFBE) (30 mg, 0.04 mmol), 1,3,5-benzenetricarboxylic acid trihydrazide (BTCH) (13.4 mg, 0.05 mmol) anhydrous mesitylene (1.5 mL), 1,4-dioxane (1.5 mL) were charged in 10 mL vial. The vial was sonicated for several minutes to get a homogeneous solution. Then 0.2 mL of 6 M acetic acid was added. Simultaneously stirring and Ar gas bubbling were maintained for a few minutes then at once closed the vial. The vial was then kept in monitored oven at 120 °C for 72 hours. After that material was removed and left undisturbed at ambient temperature for cooling. The final resulting solid was washed with anhydrous THF, acetone, CH_3OH, and 1,4-dioxane then put in a vacuum dry oven at 60 °C for one day to attain as yellow color powder.

The elemental analysis was used to determine the **H-COP** carbon (C), hydrogen (H) and nitrogen (N) contents. The observed values of C (69.61%), N (7.88%) and H (5.10%) were comparable with corresponding theoretical values (70.15%, 13.36% and 5.05%).

Nitro-explosives sensing. In this sensing arrangement, 96 μg of **H-COP** was added into 3 mL quartz cuvette containing DMF then sonication was applied for achieving homo disperse suspension (32 μg mL^{-1}). Dispersing property of the **H-COP** will smooth vicinal interaction among polymer and explosives. The fluorescence intensity measurement was performed at 500 nm upon excitation at 378 nm, while the sensing phenomenon was observed *via* explosives sequential addition (70 μL each time) from the stock solution (5.0×10^{-6} M). All sensing experiments were repeated thrice and steady results were stated.

Results and discussion

The synthesis assembly has been described in Scheme 1. The porous luminescent (**H-COP**) successfully synthesized *via* condensation reaction of 1,1,2,2-tetrakis(4-formyl-(1,1′-biphenyl))ethane (TFBE) and 1,3,5-benzenetricarboxylic acid trihydrazide (BTCH).

In polymer skeleton, monomers condensation reaction confirmation and imine linkage primarily determined through Fourier transform-infrared spectroscopy (FT-IR). There is a solid band around 1695 cm^{-1} endorsed to the aldehyde (C=O) stretching vibrations (Fig. 1a), while an adjacent strong band around 3400–3300 cm^{-1} correspond to the vibration band of amines (Fig. 1b).[46] In this **H-COP** framework, the absence of NH_2 group and C=O well stretching bands, while imine (C=N) vibrational stretching band presence at 1610 cm^{-1}, shows the reaction completion indication among both monomers. Condensation of monomers happens effectively, but still a very small band around 1650 cm^{-1} is observable, attributed to the certain unreacted aldehydes in the COP setup (Fig. 1c). According to literature studies, the **H-COP** also possess a one

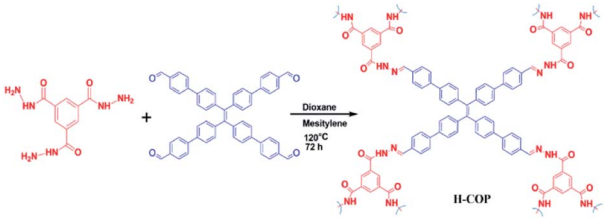

Scheme 1 The H-COP synthesis assembly.

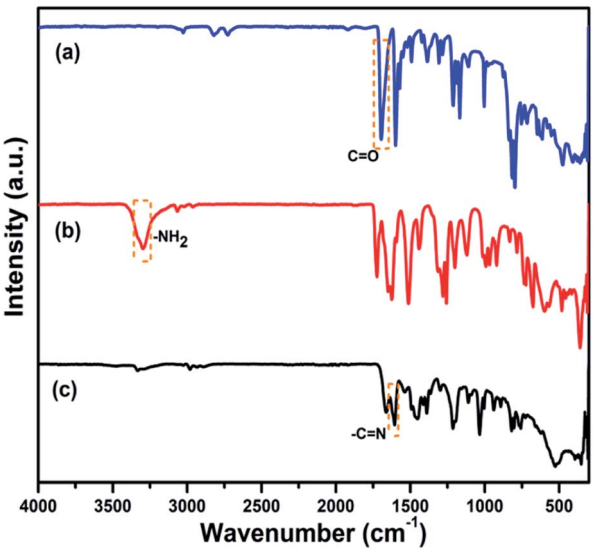

Fig. 1 FT-IR spectra (a) 1,1,2,2-tetrakis(4-formyl-(1,1′-biphenyl)) ethane (TFBE) (b) 1,3,5-benzenetricarboxylic acid trihydrazide (BTCH) and (c) H-COP.

wide diffraction peak in PXRD spectrum at 20°, shows the low crystallinity of the framework (Fig. S1†).[36,47,48]

The **H-COP** synthesis further validation was carried through ^{13}C CP/MAS solid-state NMR spectroscopy. The ^{13}C NMR spectrum shows imine carbon typical resonance signal around 156 ppm, which also confirms the bond formation among both monomers. Correspondingly, C═O bond minor chemical shift can be observed around 192 ppm (Fig. S2†). This validates unreacted groups in the polymer setup, which may cause defects in the chemical structure. For AIE property investigation, fluorescence and UV-visible experiments were carried out in DMF with increased fractions of water.[49–52] There is no obvious change in absorption and emission spectra of **H-COP** after addition of different fractions of water (Fig. S3†). The pH of **H-COP** was measured before and after the addition of water in the DMF solution, which changed from 6 to 7. The photophysical features study shows that **H-COP** has no AIE effect. The luminogenic status of **H-COP** was also investigated after exposure to different solvents for one week. There is a slight difference in fluorescence peak heights even after one week of treatment in different chemical environments (Fig. S4†). The **H-COP** permanent porosity was observed through N_2 sorption analysis at 77 K. The pore size distribution analysis of **H-COP** was measured through non-local density functional theory (NLDFT).[53–55] The **H-COP** experimental pore sizes were centered at 0.755 nm and 1.919 nm, correspond to micro-pores (Fig. 2b). Afterwards, the method of Barrett, Joyner and Halenda (BJH) applied to endorse the micro-pores existence and displays worthy consent with pore size calculation *via* NLDFT method. The **H-COP** surface area was determined *via* BET model. The **H-COP** experimentally calculated surface area is 164 $m^2\ g^{-1}$, indicates the porous framework (Fig. 2a).

The common characterization techniques scanning electron microscopy (SEM) and transmission electron microscopy (TEM)

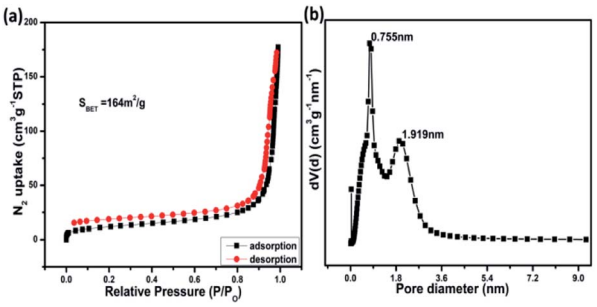

Fig. 2 The H-COP (a) N_2 sorption isotherms and (b) pore size distribution calculation.

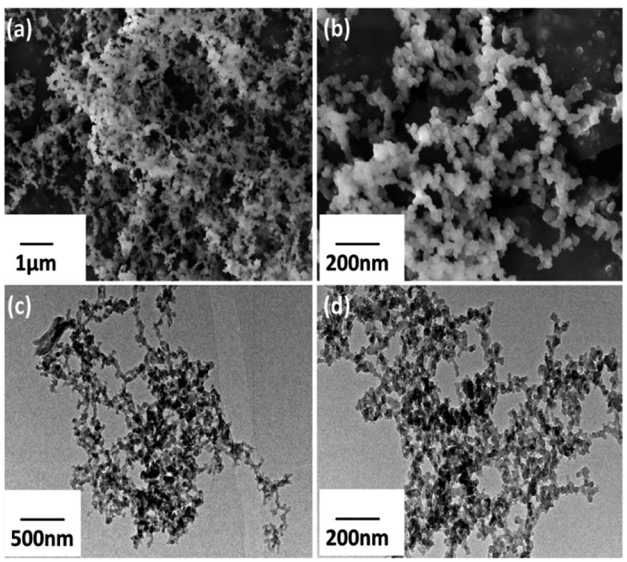

Fig. 3 (a–d) The H-COP Different magnification SEM, TEM images.

were used to expose **H-COP** surface morphology. Different magnification images were used to explain the morphology of the **H-COP**. The **H-COP** lower and higher magnification images of SEM and TEM display identical porous nano-scale structure with average size of 15–25 nm (Fig. 3a–d).

Stability

In order to investigate the **H-COP** chemical stability, the **H-COP** material was exposed to different chemical environments for more than one week including open-air, different solvents (acetonitrile, ethanol, HCl (3 M), HNO_3 (3 M) and tetrahydrofuran), different temperatures and pH, then run for FT-IR analysis. The FT-IR chemical studies show that all the peaks possess unaltered positions and imine bond (C═N) except for higher basic pH and HNO_3 acid which shows slight imine bond peaks. The **H-COP** is chemically stable and retains its unique porous structure even after treatment with different environments (Fig. S5a–c†). The **H-COP** possesses a low crystalline structure; hence, PXRD measurements were not performed for these different environments. To examine the **H-COP** thermal

stability, thermo-gravimetric (TGA) analysis and heating at different temperatures was conducted. The TGA profile of **H-COP** shows the thermal stability up to 300 °C, and loss of weight mainly occurs around 400 °C because of framework decay or carbonization (Fig. S6†), while spectra measured at different heating temperatures also shows that **H-COP** starts losing some peaks at elevated temperatures and endows that high temperature analysis destroy this framework.

Nitro-explosives sensing study

The hydrazone and aldehyde units based luminescent **H-COP** provides fluorescent channels enrich with π-electrons and act as an exceptional fluorescent sensor. The hydrazone unit possesses favorable complementary hydrogen-bonding active sites for guest probe molecules. These kind of binding interactions can aid in fluorescence-quenching phenomenon and contribute to host guest probes selective sensing.[46,56] Similarly aldehyde and hydrazone units provide platform for different interactions like π–π, electron transfer and energy transfer. Such important features of **H-COP** encourage us to investigate the sensing properties of explosives. Picric acid (PA), 4-nitrophenol (4-NP), 1,3-dinitrobenzene (DNB), and 2,4-dinitrotoluene (DNT) were chosen to examine **H-COP** sensing capability towards common explosives. Due to the well dispersion of polymer and selected explosives good solubility, all the sensing experiments were carried out in the DMF media. A suitable excitation wavelength 378 nm was selected for the **H-COP** through spectrophotometer. At ambient conditions, the **H-COP** luminescence spectra show intense emission centered at 500 nm when excited by 378 nm UV-light. The **H-COP** detection behavior was investigated *via* luminescence-quenching titration phenomenon with explosives addition each time (70 μL) to the **H-COP** suspension Fig. 4a–d, S9 & S10.† Hence proves that **H-COP** fluorescence intensity depends mainly on the concentration of the analyte; the **H-COP** fluorescence intensity decreases as the nitro explosives concentration increases.

Moreover, for various nitro explosive analytes, the quenching response also varies.

The quenching mechanism for this COP was explained *via* Stern–Volmer equation $(I_0/I) = 1 + K_{sv}[Q]$, while $K_{sv} = K_q\ \tau_0$.[57] Here I_0 and I indicate probe luminescence intensities, before and after addition of quenching analyte, K_{sv} indicates Stern–Volmer constant (M^{-1}) while [Q] stands for molar concentration of quenching analyte, K_q denotes quenching constant ($M^{-1}\ s^{-1}$) and τ_0 is the lifetime of excited state fluorescence without quenching probe. For Stern–Volmer graph, if the relationship between I_0/I and [Q] comes linear, then the value of K_{sv} is calculated from the slope value. Most of the cases, the relationship between I_0/I and [Q] possess linear deviation. The linear S–V plot suggests quenching mechanism is dynamic while deviation from linearity suggests that either its static quenching or simultaneously combination of the static and dynamic quenching.[58] During static mechanism of quenching, complex formation arises among quenching analyte and sensor probes in ground state, while the transfer of electron takes place between quenching probes and sensors in the excited state during dynamic quenching.[59] As presented above, at different concentration attained S–V graph shows very slight non-linear behavior and suggests involvement of either energy or electron transfer.

As shown above in Fig. 4a–d, S9 & S10,† the K_{sv} values were calculated by general Stern–Volmer equation. The calculated K_{sv} values for PA, P-NP, 1,3-DNB, and 2,4-DNT are 2.5×10^6, 3.8×10^6, 2.1×10^6 and 1.5×10^6, respectively. The sensitivity has direct relationship with K_{sv} and K_q values. If the K_{sv} value is larger, then it shows greater sensitivity and more interactions among the **H-COP** and nitro-explosive analytes. The calculated K_q values for PA, 4-NP, DNB, and DNT are given 0.94×10^{15}, 1.43×10^{15}, 0.79×10^{15} and 0.56×10^{15}, respectively. The obtained higher K_q value assures higher quenching rate for COP sensor.[60] The attained K_{sv} and K_q values for all tested common explosives are greater than reported COP based chemo-sensors till now (Tables S1 & S2†). Both cases followed the same order for K_{sv} and K_q (4-NP > PA > DNB > DNT).

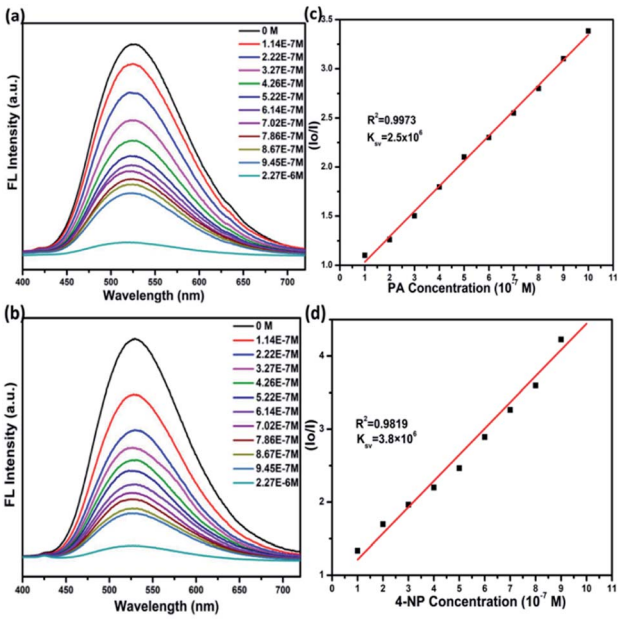

Fig. 4 H-COP luminescence-quenching titrations spectra while sequential addition (a) PA and (b) 4-NP. Stern–Volmer (S–V) plot calculations for H-COP with (c) PA and (d) 4-NP.

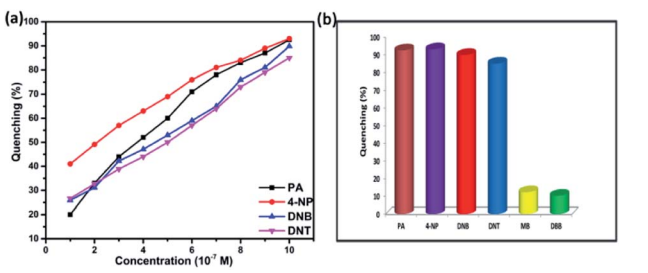

Fig. 5 The H-COP (a) quenching efficiency (%) against various concentrations of nitro explosive analytes. (b) Luminescence-quenching efficiency towards common explosives and non-explosives.

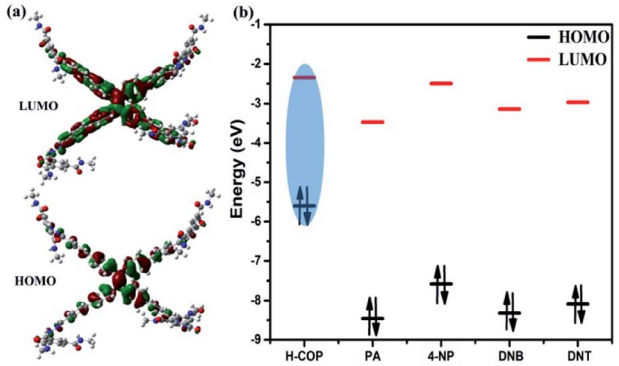

Fig. 6 (a) The H-COP HOMO–LUMO structures. (b) HOMO–LUMO calculations for H-COP and nitro-explosives.

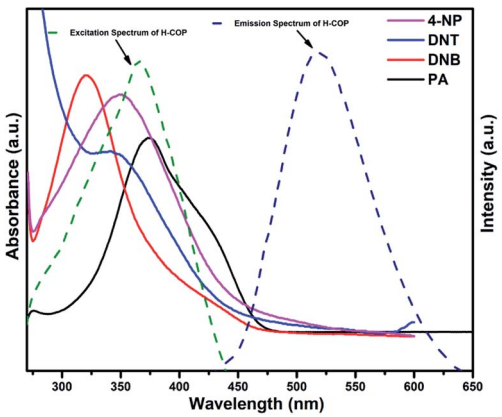

Fig. 7 The UV-vis spectra of PA, 4-NP, DNT and 4-NP and excitation & emission spectra of H-COP.

The **H-COP** structure is more selective towards nitrophenolic compounds than other common explosives and non-explosives. The reason is the existence of hydrogen-bonding among guest explosive analytes hydroxyl group, and imine bond of **H-COP**. This kind of ground state complex formation also aids in quenching.[61] Remarkably, our luminescent material shows fascinating and comparable sensitivity values for PA and 4-NP among previously reported polymer sensors. Furthermore, the detection limit was obtained *via* IUPAC recommended method (3σ/slope). Here (σ) represents standard deviation and assessed through blank sample **H-COP**/DMF suspension fluorescence intensity, while slope (m) value was determined *via* fluorescence intensity calibration curve against nitro explosive different concentrations (Fig. S7–S10†). Extraordinarily, the **H-COP** detection limit in DMF solution for PA, P-NP, DNB, and DNT is able to reach 0.17, 0.13, 0.18, and 0.25 μM, respectively.

In order to explain the **H-COP** sensing selectivity, the quenching efficiency against common nitro-explosives and non-explosives were also tested at different concentrations 2.27×10^{-6} M to 2.27×10^{-4} M, wherein the quenching % calculations were done through

$$\text{Quenching}\% = (I_0 - I)/I_0 \times 100$$

given equation.[23]

As discussed above I_0 and I represent probe luminescent intensities, calculated before and after quencher analytes addition. The non-explosive aromatic compounds concentration was adjusted 100 times greater than explosive aromatic compounds. As demonstrated above nitro explosives sequential addition to the **H-COP**/DMF suspension causes obvious reduction in the luminescence intensities of **H-COP**. Therefore, quenching percentage increases with the increasing nitro-explosive compounds concentration PA (92.50%), 4-NP (93.07%), DNB (89.84%), and DNT (85.0%) (Fig. 5a and b).

However, similar conditions non-explosive aromatic compounds addition (1.14×10^{-5} M to 2.27×10^{-4} M) to the suspension of **H-COP**/DMF, very slight change occurs (Fig. S11†). The calculated quenching % for dibromo-benzene (DBB) and methyl benzene (MB) was 10% and 12.2%, respectively (Fig. 5b), which demonstrates **H-COP** shows more attractive quenching efficiency towards explosive analytes over non-explosive analytes.

The **H-COP** effective quenching response may be due to electron enrich core ability to transfer electrons, the ability of nitro explosives to absorb energy and host–guest attraction forces. In particular, the well conjugated structure of aldehyde units facilitates nitro explosives quenching *via* π–π stacking interactions in a well-ordered system.[62] The attained results showed that **H-COP** provides a unique chemo-sensor platform, where aldehyde units and imine binding sites work synergistically to achieve greater selectivity and sensitivity towards dangerous nitro explosives.

To validate the quenching phenomenon, the **H-COP** fluorescence decay was investigated at room temperature with and without quenching probe at 500 nm while using excitation wavelength 378 nm (Fig. S12†). The calculated decay time of the **H-COP** was 2.65 ns. Moreover, the average lifespan decay of **H-COP** after addition of different quenchers PA, 4-NP, 1,3-DNB, and 2,4-DNT (5.22×10^{-7} M, 350 μL from stock solution) reduces to 2.02, 1.81, 1.72, and 1.73 ns, respectively, which indicates typical dynamic quenching for **H-COP** (Table S3†).

The theoretical calculations for **H-COP** and selected nitro-explosives were also explored to validate the mechanism through Gaussian 09W (Fig. 6b).[63] The effective quenching happens, when the framework conduction band is at a higher energy level than the LUMOs of the quenching analytes (Table S4†).[64–67] DFT calculations for **H-COP** show that excited electrons transferred from the conduction band of **H-COP** to the LUMOs of the nitro-explosives.

On the other hand, the fluorescence resonance energy transfer (FRET) hardly contributes towards quenching because of the less overlap between nitro-explosives absorption spectrums and the emission spectrum of the **H-COP** (Fig. 7),[68] while the electron transfer enhances the quenching rate due to association of the quencher and the **H-COP**. In addition, very slight non-linear quenching graphs also depict a little existence of fluorescence resonance energy transfer (FRET) (Fig. 4c, d, S9b & S10b†). Hence, from the above investigations, it is clear that the PET process is more dominant in the quenching mechanism.[69–71]

Conclusions

In this contribution, 1,1,2,2-tetrakis(4-formyl-(1,1′-biphenyl)) ethane (TFBE) and 1,3,5-benzenetricarboxylic acid trihydrazide (BTCH) monomers were chosen to build a novel luminescent polymer (**H-COP**) *via* typical Schiff-base condensation reaction. The **H-COP** material shows greater sensitivity for PA, 4-NP, 1,3-DNB, and 2,4-DNT with detection limit 0.17, 0.13, 0.18, and 0.25 μM, respectively. In addition, the **H-COP** displays exceptionally great selectivity for common nitro explosive compounds over non-explosive compounds. The quenching mechanism shows that the PET process is more dominant over the RET. Under similar conditions, the **H-COP** till now is superior to the formerly reported polymer luminescent based sensors. This investigation provides capable strategy for developing luminescent porous polymers with excellent potential for nitro-explosives detection.

Conflicts of interest

The authors declare no conflict of interest.

Acknowledgements

This work was supported by the National Natural Science Foundation of China (No. 92061201, 21825106, 21901234, 21905254), NSFC-Henan Joint Foundation (U12004190), the Program for Innovative Research Team (in Science and Technology) in Universities of Henan Province (19IRTSTHN022), the Central Plains Academician Fund of Henan Province (No. 22180017), the Key Scientific and Technological Project of Henan Province (202102210027) and Zhengzhou University.

References

1 X. Sun, Y. Wang and Y. Lei, Fluorescence based explosive detection: from mechanisms to sensory materials, *Chem. Soc. Rev.*, 2015, **44**, 8019–8061.
2 M. S. Meaney and V. L. McGuffin, Luminescence-based methods for sensing and detection of explosives, *Anal. Bioanal. Chem.*, 2008, **391**, 2557–2576.
3 W. J. Peveler, A. Roldan, N. Hollingsworth, M. J. Porter and I. P. Parkin, Multichannel detection and differentiation of explosives with a quantum dot array, *ACS Nano*, 2016, **10**, 1139–1146.
4 N. Akhtar, S. A. El-Safty, M. Khairy and W. A. El-Said, Fabrication of a highly selective nonenzymatic amperometric sensor for hydrogen peroxide based on nickel foam/cytochrome c modified electrode, *Sens. Actuators, B*, 2015, **207**, 158–166.
5 M. Baghayeri, H. Alinezhad, M. Fayazi, M. Tarahomi, R. Ghanei-Motlagh and B. Maleki, A novel electrochemical sensor based on a glassy carbon electrode modified with dendrimer functionalized magnetic graphene oxide for simultaneous determination of trace Pb(II) and Cd(II), *Electrochim. Acta*, 2019, **312**, 80–88.
6 M. A. Farea, H. Y. Mohammed, S. M. Shirsat, P. W. Sayyad, N. N. Ingle, T. Al-Gahouari, M. M. Mahadik, G. A. Bodkhe and M. D. Shirsat, Hazardous gases sensors based on conducting polymer composites, *Chem. Phys. Lett.*, 2021, **776**, 138703.
7 S. S. Nagarkar, B. Joarder, A. K. Chaudhari, S. Mukherjee and S. K. Ghosh, Highly selective detection of nitro explosives by a luminescent metal–organic framework, *Angew. Chem.*, 2013, **125**, 2953–2957.
8 M. E. Germain and M. J. Knapp, Optical explosives detection: from color changes to fluorescence turn-on, *Chem. Soc. Rev.*, 2009, **38**, 2543–2555.
9 K.-S. Ju and R. E. Parales, Nitroaromatic compounds, from synthesis to biodegradation, *Microbiol. Mol. Biol. Rev.*, 2010, **74**, 250–272.
10 X. Tian, L. Chen, X. Qing, K. Yu, X. Wang and X. Wang, Hybrid cadmium tellurium quantum dots for rapid visualization of trace-level nitroaromatic explosives, *Anal. Lett.*, 2014, **47**, 2035–2047.
11 N. N. Perreault, D. Manno, A. Halasz, S. Thiboutot, G. Ampleman and J. Hawari, Aerobic biotransformation of 2,4-dinitroanisole in soil and soil Bacillus sp, *Biodegradation*, 2012, **23**, 287–295.
12 E. Hussain, Y. Li, C. Cheng, H. Zhuo, S. A. Shahzad, S. Ali, M. Ismail, H. Qi and C. Yu, Benzo [ghi] perylene and coronene as ratiometric fluorescence probes for the selective sensing of nitroaromatic explosives, *Talanta*, 2020, **207**, 120316.
13 R. L. Marple and W. R. LaCourse, Application of photoassisted electrochemical detection to explosive-containing environmental samples, *Anal. Chem.*, 2005, **77**, 6709–6714.
14 K. J. Indest, S. J. Everman, J. H. Lindsay, C. M. Jung, J. C. Smith and S. B. Newell, Effects of acute exposures of 2,4,6-trinitrotoluene and inorganic lead on the fecal microbiome of the green anole (*Anolis carolinensis*), *PLoS One*, 2018, **13**, e0208281.
15 L. C. Bartel, M. M. de Mecca and J. A. Castro, Nitroreductive metabolic activation of some carcinogenic nitro heterocyclic food contaminants in rat mammary tissue cellular fractions, *Food Chem. Toxicol.*, 2009, **47**, 140–144.
16 M. Cerruti, J. Jaworski, D. Raorane, C. Zueger, J. Varadarajan, C. Carraro, S.-W. Lee, R. Maboudian and A. Majumdar, Polymer-oligopeptide composite coating for selective detection of explosives in water, *Anal. Chem.*, 2009, **81**, 4192–4199.
17 Y. Salinas, R. Martínez-Máñez, M. D. Marcos, F. Sancenón, A. M. Costero, M. Parra and S. Gil, Optical chemosensors and reagents to detect explosives, *Chem. Soc. Rev.*, 2012, **41**, 1261–1296.
18 J. Moros and J. J. Laserna, New Raman–laser-induced breakdown spectroscopy identity of explosives using parametric data fusion on an integrated sensing platform, *Anal. Chem.*, 2011, **83**, 6275–6285.
19 K. E. Brown, M. T. Greenfield, S. D. McGrane and D. S. Moore, Advances in explosives analysis—part I:

animal, chemical, ion, and mechanical methods, *Anal. Bioanal. Chem.*, 2016, **408**, 35–47.
20 D. S. Moore, Recent advances in trace explosives detection instrumentation, *Sens. Imag. Int. J.*, 2007, **8**, 9–38.
21 C. Yu, D. Qin, X. Jiang, X. Zheng and B. Deng, N-doped carbon quantum dots from osmanthus fragrans as a novel off-on fluorescent nanosensor for highly sensitive detection of quercetin and aluminium ion, and cell imaging, *J. Pharm. Biomed. Anal.*, 2021, **192**, 113673.
22 R. G. Ewing, D. A. Atkinson, G. Eiceman and G. Ewing, A critical review of ion mobility spectrometry for the detection of explosives and explosive related compounds, *Talanta*, 2001, **54**, 515–529.
23 M. E. Walsh, Determination of nitroaromatic, nitramine, and nitrate ester explosives in soil by gas chromatography and an electron capture detector, *Talanta*, 2001, **54**, 427–438.
24 J. M. Sylvia, J. A. Janni, J. Klein and K. M. Spencer, Surface-enhanced Raman detection of 2,4-dinitrotoluene impurity vapor as a marker to locate landmines, *Anal. Chem.*, 2000, **72**, 5834–5840.
25 Y. Zhang, X. Ma, S. Zhang, C. Yang, Z. Ouyang and X. Zhang, Direct detection of explosives on solid surfaces by low temperature plasma desorption mass spectrometry, *Analyst*, 2009, **134**, 176–181.
26 R. Luggar, M. Farquharson, J. Horrocks and R. Lacey, Multivariate analysis of statistically poor EDXRD spectra for the detection of concealed explosives, *X-Ray Spectrom.*, 1998, **27**, 87–94.
27 S. F. Hallowell, Screening people for illicit substances: a survey of current portal technology, *Talanta*, 2001, **54**, 447–458.
28 Y.-w. Wu, A.-j. Qin and B. Z. Tang, AIE-active polymers for explosive detection, *Chin. J. Polym. Sci.*, 2017, **35**, 141–154.
29 M. S. Meaney and V. L. McGuffin, Investigation of common fluorophores for the detection of nitrated explosives by fluorescence quenching, *Anal. Chim. Acta*, 2008, **610**, 57–67.
30 P. Shaw and P. Burn, Real-time fluorescence quenching-based detection of nitro-containing explosive vapours: what are the key processes?, *Phys. Chem. Chem. Phys.*, 2017, **19**, 29714–29730.
31 A. Lan, K. Li, H. Wu, D. H. Olson, T. J. Emge, W. Ki, M. Hong and J. Li, A luminescent microporous metal–organic framework for the fast and reversible detection of high explosives, *Angew. Chem.*, 2009, **121**, 2370–2374.
32 Q. Zhou and T. M. Swager, Method for enhancing the sensitivity of fluorescent chemosensors: energy migration in conjugated polymers, *J. Am. Chem. Soc.*, 1995, **117**, 7017–7018.
33 S. J. Toal and W. C. J. Trogler, Polymer sensors for nitroaromatic explosives detection, *J. Mater. Chem.*, 2006, **16**, 2871–2883.
34 Z. Zhao, X. Song, L. Liu, G. Li, S. Shah and C. Hao, A recognition mechanism study: Luminescent metal-organic framework for the detection of nitro-explosives, *J. Mol. Graphics Modell.*, 2018, **80**, 132–137.
35 A. Dutta, A. Singh, X. Wang, A. Kumar and J. Liu, Luminescent sensing of nitroaromatics by crystalline porous materials, *CrystEngComm*, 2020, **22**, 7736–7781.
36 Z. Xiang and D. Cao, Synthesis of luminescent covalent–organic polymers for detecting nitroaromatic explosives and small organic molecules, *Macromol. Rapid Commun.*, 2012, **33**, 1184–1190.
37 A. Buragohain and S. Biswas, Cerium-based azide-and nitro-functionalized UiO-66 frameworks as turn-on fluorescent probes for the sensing of hydrogen sulphide, *CrystEngComm*, 2016, **18**, 4374–4381.
38 Y. Yuan, H. Ren, F. Sun, X. Jing, K. Cai, X. Zhao, Y. Wang, Y. Wei and G. Zhu, Sensitive detection of hazardous explosives *via* highly fluorescent crystalline porous aromatic frameworks, *J. Mater. Chem.*, 2012, **22**, 24558–24562.
39 M. Asad, S. Wang, Q.-Y. Wang, L. Li, M. I. Anwar, A. Younas and S.-Q. Zang, Aqueous media ultra-sensitive detection of antibiotics *via* highly stable luminescent 3D Cadmium-based MOF, *New J. Chem.*, 2021, **45**, 20887–20894.
40 Q. Gao, X. Li, G.-H. Ning, K. Leng, B. Tian, C. Liu, W. Tang, H.-S. Xu and K. P. Loh, Highly photoluminescent two-dimensional imine-based covalent–organic frameworks for chemical sensing, *Chem. Commun.*, 2018, **54**, 2349–2352.
41 M. S. Lohse and T. Bein, Covalent–organic frameworks: structures, synthesis, and applications, *Adv. Funct. Mater.*, 2018, **28**, 1705553.
42 S. Dalapati, S. Jin, J. Gao, Y. Xu, A. Nagai and D. Jiang, An azine-linked covalent–organic framework, *J. Am. Chem. Soc.*, 2013, **135**, 17310–17313.
43 X. Liu, B. Liu, G. Li and Y. Liu, Two anthracene-based metal–organic frameworks for highly effective photodegradation and luminescent detection in water, *J. Mater. Chem. A*, 2018, **6**, 17177–17185.
44 K. R. Ghosh, S. K. Saha and Z. Y. Wang, Ultra-sensitive detection of explosives in solution and film as well as the development of thicker film effectiveness by tetraphenylethene moiety in AIE active fluorescent conjugated polymer, *Polym. Chem.*, 2014, **5**, 5638–5643.
45 R. Xue, H. Guo, T. Wang, L. Gong, Y. Wang, J. Ai, D. Huang, H. Chen and W. Yang, Fluorescence properties and analytical applications of covalent organic frameworks, *Anal. Methods*, 2017, **9**, 3737–3750.
46 M. Faheem, S. Aziz, X. Jing, T. Ma, J. Du, F. Sun, Y. Tian and G. Zhu, Dual luminescent covalent organic frameworks for nitro-explosive detection, *J. Mater. Chem. A*, 2019, **7**, 27148–27155.
47 Y. Zhuang, H. Shan, Z. Zhang, S. Li, Q. Zhu, Z. Si, S. Yang, Z. Yang, D. Cai and P. Qin, Triazine-based covalent–organic polymer as stable luminescent probe for highly selective detection of 2, 4, 6-trinitrophenol, *Dyes Pigm.*, 2021, **192**, 109421.
48 L. Guo and D. Cao, Color tunable porous organic polymer luminescent probes for selective sensing of metal ions and nitroaromatic explosives, *J. Mater. Chem. C*, 2015, **3**, 8490–8494.

49 X. Wang, G. Ding, Y. Duan, Y. Zhu, G. Zhu, M. Wang, X. Li, Y. Zhang, X. Qin and C.-H. Hung, A novel triphenylamine-based bis-Schiff bases fluorophores with AIE-Activity as the hydrazine fluorescence turn-off probes and cell imaging in live cells, *Talanta*, 2020, **217**, 121029.

50 Y. Liu, J. Nie, J. Niu, F. Meng and W. Lin, Ratiometric fluorescent probe with AIE property for monitoring endogenous hydrogen peroxide in macrophages and cancer cells, *Sci. Rep.*, 2017, **7**, 1–10.

51 X. Ma, J. Yue, B. Qiao, L. Zhou, Y. Gao, Y. Wang, Y. Lai, Y. Geng, E. Feng and M. Liu, Regulation of the bi-color fluorescence changes of AIE supramolecular self-assembly gels by interaction with Al 3+ and energy transfer, *Mat.adv.*, 2021, **2**, 6075–6082.

52 G. Ding, X. Wang, W. Zhao, S. Mao, J. Wang, S. Kang, J. Meng, H. Liu, H. Yang and S. Liang, A portable AIEgen-based organic fluorescence sensor design and its reusable application in information storage and pH detection, *Tetrahedron*, 2021, 132258.

53 A. V. Neimark, Y. Lin, P. I. Ravikovitch and M. Thommes, Quenched solid density functional theory and pore size analysis of micro-mesoporous carbons, *Carbon*, 2009, **47**, 1617–1628.

54 J. Landers, G. Y. Gor and A. V. Neimark, Density functional theory methods for characterization of porous materials, *Colloids Surf., A*, 2013, **437**, 3–32.

55 E. Ustinov, D. Do and V. Fenelonov, Pore size distribution analysis of activated carbons: Application of density functional theory using nongraphitized carbon black as a reference system, *Carbon*, 2006, **44**, 653–663.

56 N. Huang, P. Wang and D. Jiang, Covalent organic frameworks: a materials platform for structural and functional designs, *Nat. Rev. Mater.*, 2016, **1**, 1–19.

57 L. Yang, Y.-L. Liu, C.-G. Liu, F. Ye and Y. Fu, A luminescent sensor based on a new Cd-MOF for nitro explosives and organophosphorus pesticides detection, *Inorg. Chem. Commun.*, 2020, **122**, 108272.

58 Y. Yang, L. Zhao, M. Sun, P. Wei, G. Li and Y. Li, Highly sensitive luminescent detection toward polytypic antibiotics by a water-stable and white-light-emitting MOF-76 derivative, *Dyes Pigm.*, 2020, **180**, 108444.

59 S. M. Aly, M. R. Parida, E. Alarousu and O. F. Mohammed, Ultrafast electron injection at the cationic porphyrin–graphene interface assisted by molecular flattening, *Chem. Commun.*, 2014, **50**, 10452–10455.

60 Q. Zhang, M. Lei, J. Zhang and Y. Shi, A luminescent 3D Zn(II)-organic framework showing fast, selective and reversible detection of p-nitrophenol in aqueous media, *J. Lumin.*, 2016, **180**, 287–291.

61 T. Fujii, M. Sano, S. Mishima and H. Hiratsuka, Fluorescence quenching of fluorenone by alcohols, *Bull. Chem. Soc. Jpn.*, 1996, **69**, 1833–1839.

62 S. Shaligram, P. P. Wadgaonkar and U. K. Kharul, Fluorescent polymeric ionic liquids for the detection of nitroaromatic explosives, *J. Mater. Chem. A*, 2014, **2**, 13983–13989.

63 A. Frisch, *Gaussian 09W Reference*, Willingford, USA, 25p, 2009.

64 N. Goel and N. Kumar, A dual-functional luminescent Tb (III) metal–organic framework for the selective sensing of acetone and TNP in water, *RSC Adv.*, 2018, **8**, 10746–10755.

65 G.-Y. Wang, C. Song, D.-M. Kong, W.-J. Ruan, Z. Chang and Y. Li, Two luminescent metal–organic frameworks for the sensing of nitroaromatic explosives and DNA strands, *J. Mater. Chem. A*, 2014, **2**, 2213–2220.

66 X. Zhou, H. Li, H. Xiao, L. Li, Q. Zhao, T. Yang, J. Zuo and W. Huang, A microporous luminescent europium metal–organic framework for nitro explosive sensing, *Dalton Trans.*, 2013, **42**, 5718–5723.

67 G.-D. Wang, Y.-Z. Li, W.-J. Shi, B. Zhang, L. Hou and Y.-Y. Wang, A robust cluster-based Eu-MOF as multi-functional fluorescence sensor for detection of antibiotics and pesticides in water, *Sens. Actuators, B*, 2021, **331**, 129377.

68 X. G. Liu, C. L. Tao, H. Q. Yu, B. Chen, Z. Liu, G. P. Zhu and B. Z. Tang, A new luminescent metal–organic framework based on dicarboxyl-substituted tetraphenylethene for efficient detection of nitro-containing explosives and antibiotics in aqueous media, *J. Mater. Chem. C*, 2018, **6**(12), 2983–2988.

69 A. Sharma, D. Kim, J.-H. Park, S. Rakshit, J. Seong, G. H. Jeong, O.-H. Kwon and M. S. Lah, Mechanistic insight into the sensing of nitroaromatic compounds by metal-organic frameworks, *Commun. Chem.*, 2019, **2**, 1–8.

70 M. R. Eslami and N. Alizadeh, Ultrasensitive and selective QCM sensor for detection of trace amounts of nitroexplosive vapors in ambient air based on polypyrrole—Bromophenol blue nanostructure, *Sens. Actuators, B*, 2019, **278**, 55–63.

71 L. Yang, Y.-L. Liu, C.-G. Liu, Y. Fu and F. Ye, A built-in self-calibrating luminescence sensor based on RhB@Zr-MOF for detection of cations, nitro explosives and pesticides, *RSC Adv.*, 2020, **10**, 19149–19156.